Scintillation, dosimeter and optical properties of MgF_2 transparent ceramics doped with Gd^{3+}

Fumiya Nakamura[a,*], Takumi Kato[a], Go Okada[a], Naoki Kawano[a], Noriaki Kawaguchi[a], Kentaro Fukuda[b], Takayuki Yanagida[a]

[a] Nara Institute of Science and Technology (NAIST), 8916-5 Takayama-cho, Ikoma-shi, Nara 630-0192, Japan
[b] Tokuyama Corporation, 1-1 Mikage-cho, Shunan-shi, Yamaguchi 745-8648, Japan

ARTICLE INFO

ABSTRACT

In this study, we have developed MgF_2:Gd transparent ceramics by spark plasma sintering (SPS) and evaluated the scintillation, dosimeter and optical properties. All the sample were successfully synthesized in a transparent form with relative densities over 99% to that of the single crystal. The samples were confirmed to show scintillation, thermally-stimulated luminescence (TSL) and optically-stimulated luminescence (OSL). The origin of these emissions was due to the 4f-4f transitions of Gd^{3+} appearing as a single peak at 310 nm. In particular, the TSL was very sensitive to X-rays, and especially the 1% Gd-doped sample showed a sensitivity as low as 0.1 mGy. The TSL response increases monotonically with the irradiation dose, and the dynamic range was confirmed to be over 0.1–1000 mGy, which was equivalent sensitivity to that of commercial personal dosimeters.

1. Introduction

Ionizing radiation detectors are mainly classified into two types. One is a direct conversion type, which directly converts radiations to electrical signals. An example is semiconductor devices using Si, Ge, Se, and CdTe. The other is an indirect conversion type, which often uses phosphors to convert radiation to light, and the light is further converted to electrical signals by photodetectors such as photomultiplier tubes (PMTs) in general. Phosphors used in the indirect conversion detectors are often referred as scintillators and dosimeters depending on the mechanisms involved and applications. Scintillators almost instantly convert absorbed energy of ionizing radiation into numerous number of low energy photons, and they are widely used in various fields such as high energy physics [1], security [2] and medicine [3]. On the other hand, dosimeters store and accumulate incident radiation energy for a certain period of time, which is kept in a form of charge trapping at localized sites. The trapped charges can be intentionally freed by an external stimulation of heat or light, and the charges eventually recombine to emit photons. The light emission due to heat stimulation is so-called thermally-stimulated luminescence (TSL) while that by optical stimulation is called optically stimulated luminescence (OSL). Dosimeters are mainly used in personal dose monitoring [4] and radiation imaging applications [5]. When dosimeters are used in personal dose monitoring applications, the effective atomic number (Z_{eff}) should be close to that of soft tissue of human body ($Z_{eff} = 7.51$)

because interactions of ionizing radiation with matter strongly depends on the chemical compositions. In addition, the dosimeters are also required to have a good linear response to incident radiation dose for accurate measurements. Scintillators and dosimeters have been separately studied and developed in different fields. However, it is important to investigate both scintillation and dosimeter properties together for better understandings of the luminesce mechanisms because it was recently pointed out that these two properties are complementarily related in some materials [6,7].

Fluorides are common materials for scintillators and dosimeters. For example, $LiCaAlF_6$ crystals doped with Eu^{2+} or Ce^{3+} are practical neutron scintillators and commercially available from Tokuyama Corp. [8]. Dosimeters using fluoride materials are especially well-known to show distinct TSL properties. The common examples are LiF:Ti,Mg [9], CaF_2:Dy [10] and CaF_2:Tm [11]. In addition, MgF_2 has attracted much attention as a dosimeter material because the effective atomic number ($Z_{eff} = 10.46$) is very close to that of biological tissue, although it has not been practically used yet. So far, many researchers have made efforts on investigating TSL properties of MgF_2, and it has been found out that doping with some rare earth (RE) and transitional metal ions improves the properties [12–18]. Gd is one of RE ions and has luminescence features appearing as a single narrow emission peaking at 310 nm due to the 4f-4f transitions regardless of the host material compositions [19]. The latter emission is suitable to be used with a PMT having a typical sensitivity around 300–500 nm. In addition, the emission

* Corresponding author.
  E-mail address: nakamura.fumiya.nz9@ms.naist.jp (F. Nakamura).

wavelength is short enough so the signal is less likely affected by black-body radiation from the heater when used as TSL dosimeters. In spite of the large number of earlier researches and advantages of MgF_2 as a host material and Gd ion as an activator, to the best of our knowledge, there are no research reports on any luminescence properties of Gd-doped MgF_2 transparent ceramics.

It is particularly important to use a bulk transparent material for both scintillators and dosimeters. A transparent matrix enables photons to escape effectively, so the sensitivity as a detector is enhanced. So far, bulk inorganic solids of single crystal have been mainly utilized for scintillators and dosimeters owing to their high optical qualities. However, transparent ceramics have recently attracted much attention as optical materials because they have distinct industrial advantages such as higher mechanical strength, higher uniformity and lower fabrication cost compared with single crystals. In addition, it has been reported that selected transparent ceramics showed better luminescence properties than those of single crystal form [20,21]. Spark plasma sintering (SPS) is one of sintering techniques used to fabricate transparent ceramics [22–32] and characterized by a rapid consolidation rate. In general, SPS is performed in a high reductive environment, which can effectively increase a concentration of defects responsible for dosimeter properties. For these reasons, we have synthesized MgF_2:Gd transparent ceramics using SPS and evaluated the scintillation, dosimeter and optical properties.

2. Experimental

MgF_2:Gd transparent ceramics with different concentrations (0.01, 0.1 and 1%) of Gd were synthesized by the SPS technique using Sinter Land LabX-100 in vacuum. Raw powders of MgF_2 and GdF_3 (4N; Tokuyama Corp.) were mixed by a mortar and pestle. 0.5 g of the mixture was loaded into a cylindrical graphite die with a hole of 10.4 mm in diameter and held between two graphite punches inserted in the hole. Sintering was conducted by applying pulse current while uniaxial pressure was applied through the graphite assembly. The sintering was carried out in two steps. First, the temperature was increased from the room temperature to 550 °C with a heating rate of 100 °C/min while applying 6 MPa pressure and then kept for 10 min. Next, the temperature was further increased to 750 °C with a heating rate of 100 °C/min while applying 70 MPa pressure and then kept for 7 min. A K-type thermocouple was attached onto the graphite die to observe the temperature. After the sintering, the top and bottom surfaces of the synthesized ceramic samples were mechanically polished by a polishing machine (MetaServ 250, BUEHLER). Subsequently, all the prepared samples were equally characterized by the same manner described below.

An X-ray diffraction (XRD) pattern was measured by a diffractometer (MiniFlex600, Rigaku). The diffractometer was equipped with a microfocus X-ray tube (Cu Kα) operated at 40 kV and 15 mA. The scanning 2θ range was 20–60°. Density was measured by the Archimedes method using a scale unit (GR-120 and AD-1653, A & D). In this measurement, MgF_2 single crystal (Tokuyama Corp.) was used as a reference. Optical in-line transmittance was evaluated by a spectrophotometer (V670, JASCO) over the spectral range of 190–2000 nm with 1 nm intervals. Quantaurus-QY (C11347, Hamamatsu Photonics) was used to measure PL emission and excitation spectra as well as quantum yield. Quantaurus-τ (C11367, Hamamatsu Photonics) was used to evaluate PL decay profiles monitoring at 310 nm during 265 nm excitation.

X-ray induced scintillation spectrum was evaluated by our original setup [20]. Here, an X-ray generator equipped with a W anode target (XRB80P & N200 × 4550, Spellman) and a Be window was used as an excitation source, and the X-ray generator was operated with a tube voltage of 40 kV and current of 5.2 mA. An optical fiber (2.0 m) was used to guide the scintillation photons from the sample to a CCD-based spectrometer (Andor DU-420-BU2 CCD and Shamrock 163

monochromator). The CCD detector was cooled down to 193 K by a Peltier module in order to reduce the thermal noise. An afterglow characterization system equipped with a pulse X-ray tube [33] was used to measure X-ray induced scintillation decay time profile. During the measurements, the X-ray source was supplied with the voltage of 30 kV.

TSL glow curve was measured by a TSL reader (TL-2000, Nanogray Inc.) over the temperature range of 50–490 °C with a heating rate of 1 °C/s [34]. Prior to the measurement, the sample was irradiated by X-rays with a certain dose ranging from 0.1 mGy to 1000 mGy. In order to measure TSL spectra, the TSL emission was collected by an optical fiber to guide into a spectrometer (QE Pro, Ocean Optics) while the sample was heated with a heating rate of 1 °C/s on a ceramic heater system (SCR-SHQ-A, Sakaguchi). OSL was measured under 470 nm stimulation by a spectrofluorometer (FP8600, JASCO). OSL decay profiles were also measured using the same spectrofluorometer by monitoring the emission intensity at 315 nm during a stimulation at 470 nm with a constant intensity.

3. Results and discussion

3.1. Sample

Fig. 1 shows a photograph of MgF_2:Gd transparent ceramic samples synthesized in this research. The samples were transparent enough that the black lines on the back of the samples can be seen. The thickness of the samples was fixed to 1.0 mm. Table 1 summarizes densities of the samples. The relative densities of the 0.01, 0.1 and 1% Gd-doped samples were 99.9, 99.8 and 99.3%, respectively. The relative density decreased as the concentration of Gd increased. This trend is sometimes observed in RE doped transparent ceramics sintered by SPS. It is suggested that introducing RE ions decreases the sintering kinetics, which is associated with an increase of residual porosity [35]. Fig. 2 shows XRD patterns of the samples. An impurity phase of GdF_3 was confirmed in the 1% Gd-doped sample [36]. It was suggested that some of Gd^{3+} could not replace Mg^{2+} in the 1% Gd-sample because of the large difference of ionic radius between Mg^{2+} (0.66 Å) and Gd^{3+} (0.97 Å).

3.2. Optical properties

Fig. 3 shows in-line transmittance spectra of MgF_2:Gd transparent ceramic samples with different concentrations of Gd over the wavelength range of 190–2000 nm. The transmittance decreased with increasing the concentration of Gd. This result is consistent with the results of relative density measurements since porosity is the most dominant source of scattering in transparent ceramics.

Fig. 4 shows the PL excitation/emission contour graph of MgF_2:1%Gd transparent ceramic sample as an example. Under 270 nm excitation, the samples showed a single line emission peaking at 310 nm. The origin of this emission is considered be due to the 4f-4f transitions of Gd^{3+} for its well-known spectral features [19]. The
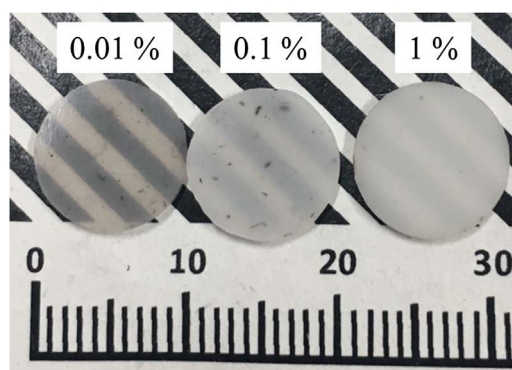
Fig. 1. Synthesized MgF_2 transparent ceramics doped with Gd^{3+} (0.01, 0.1 and 1%).

Table 1
Relative densities of MgF$_2$:Gd transparent ceramic samples with respect to that of MgF$_2$ single crystal.

	Relative density (%)
0.01% Gd	99.9
0.1% Gd	99.8
1% Gd	99.3
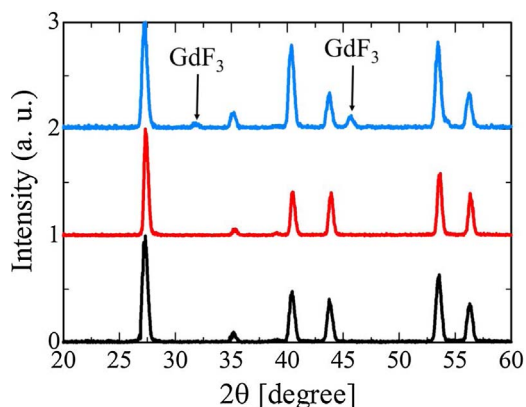
Fig. 2. 2 XRD patterns of MgF$_2$:Gd transparent ceramic samples.
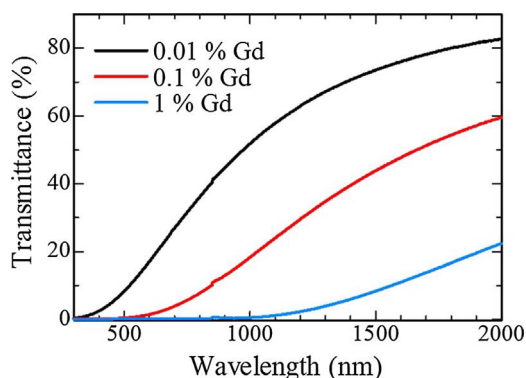
Fig. 3. Transmittance spectra of MgF$_2$:Gd transparent ceramic samples.
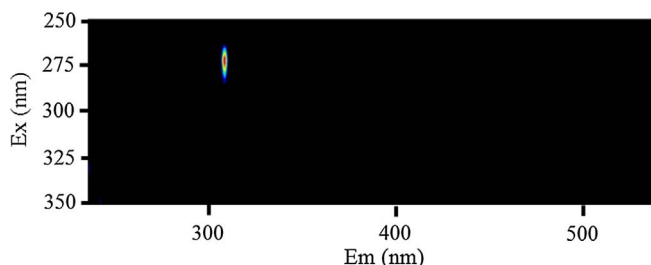
Fig. 4. Representative PL emission and excitation map of MgF$_2$:1%Gd transparent ceramic sample.

quantum yields of the 0.1 and 1% Gd-doped samples were 2 and 3%, respectively. The quantum yield of 0.01% Gd-doped sample was not measurable because the emission intensity was very low. The quantum yield increased as the concentration increased.

PL decay profiles of the MgF$_2$:Gd transparent ceramic samples are shown in Fig. 5. The excitation wavelength was 265 nm while the monitoring wavelength was 310 nm. The decay curves were well-approximated by a first-order exponential decay function. The derived decay constants of the 0.01, 0.1 and 1% Gd-doped samples were 5.90, 4.14 and 3.97 ms, respectively. These values are typical for the 4f-4f transitions of Gd^{3+} [19]. Therefore, with the results of PL spectral
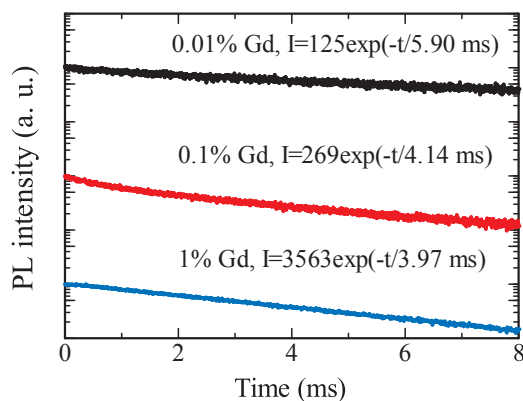
Fig. 5. PL decay profiles of MgF2:Gd transparent ceramic samples. The excitation wavelength was 265 nm while the emission wavelength monitored was 310 nm.

features, this emission was attributed to the Gd^{3+} ion due to the 4f-4f transitions. The decay time became shorter as the Gd concentration increased. This implies that non-radiative decay process due to concentration quenching is not dominant in this system, as also suggested by the results of quantum yield.

3.3. Scintillation properties

Fig. 6 shows X-ray induced scintillation spectra of MgF$_2$:Gd transparent ceramic samples. An intense peak due to the 4f-4f transitions of Gd^{3+} was observed at 310 nm, as also observed in the PL. In addition to the intense peak, a broad emission was observed around 380 nm, which was not seen in the PL measurements. This emission was attributed to the host since it was also observed in non-doped MgF$_2$ transparent ceramic [37]. The intensity increased as the Gd concentration increased, and it is the same tendency with the PL. From this result, the emission intensity of the broad peak became higher associated with Gd concentrations, which implies that the emission origin can be defects generated by charge imbalance between Mg^{2+} and Gd^{3+}.

Fig. 7 represents X-ray induced scintillation decay time profiles of the MgF$_2$:Gd transparent ceramic samples. The decay curves were well-approximated by a second-order exponential decay function. Decay times of the faster component for the 0.01, 0.1 and 1% Gd-doped samples were 245, 663 and 522 μs, respectively. These components were ascribed to the host emission around 380 nm since a similar decay time constant was reported for non-doped MgF$_2$ transparent ceramic [37]. Decay times of the slower component for the 0.01, 0.1 and 1% Gd-doped samples were 6.27, 4.29 and 4.03 ms, respectively. These values are in a typical range for the 4f-4f transitions of Gd^{3+} [19]. The decay times became shorter as the Gd concentration increased as in the PL. Despite the same origin, the scintillation decay times were slower than those of PL. The interpretation is that scintillation processes involve
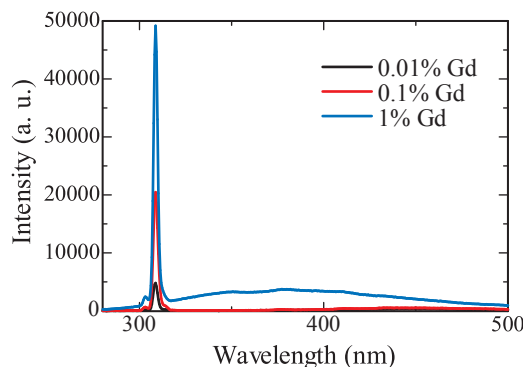
Fig. 6. X-ray induced scintillation spectra of MgF$_2$:Gd transparent ceramic samples.
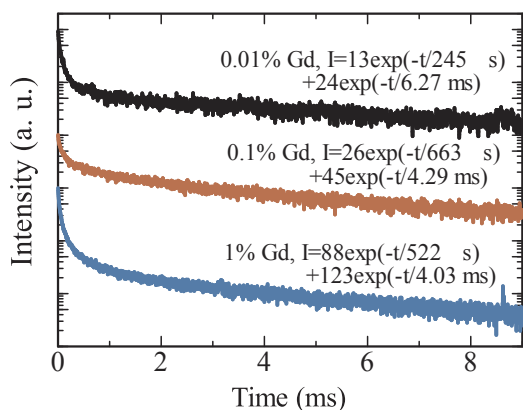
Fig. 7. Scintillation decay time profiles of MgF$_2$:Gd transparent ceramic samples.
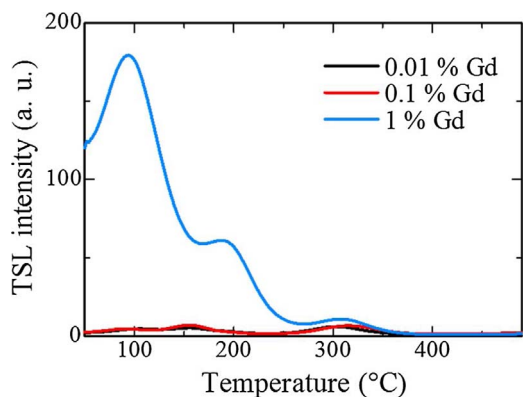
Fig. 8. TSL glow curves of MgF$_2$ transparent ceramic doped with Gd^{3+} after 1 Gy X-ray irradiation.
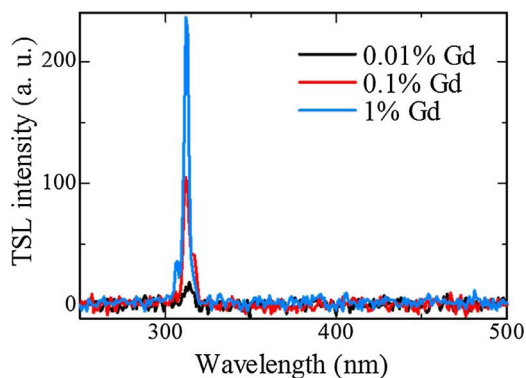
Fig. 9. TSL emission spectra of MgF$_2$ transparent ceramic doped with Gd^{3+} measured at 50–350 °C after 10 Gy X-ray irradiation.

Table 2
Derived activation energies MgF$_2$:Gd transparent ceramic samples.

	Activation energy (eV)	Frequency factor (s^{-1})
0.01% Gd, 110 °C	0.84	1.51×10^9
0.01% Gd, 200 °C	1.00	1.43×10^{10}
0.01% Gd, 300 °C	1.00	1.05×10^8
0.1% Gd, 110 °C	1.00	2.75×10^{11}
0.1% Gd, 200 °C	1.00	3.14×10^{10}
0.1% Gd, 300 °C	1.00	1.53×10^8
1% Gd, 110 °C	0.89	3.05×10^{10}
1% Gd, 200 °C	0.89	2.23×10^9
1% Gd, 300 °C	1.00	3.66×10^8
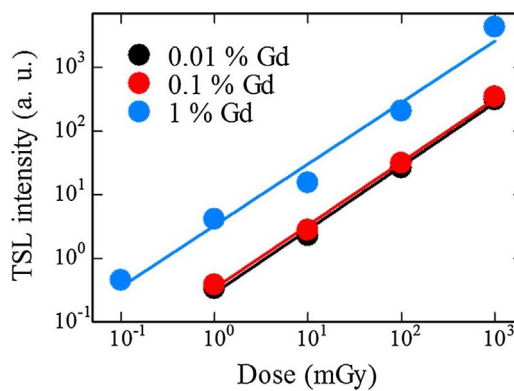
Fig. 10. TSL dose response of MgF$_2$:Gd transparent ceramic samples.
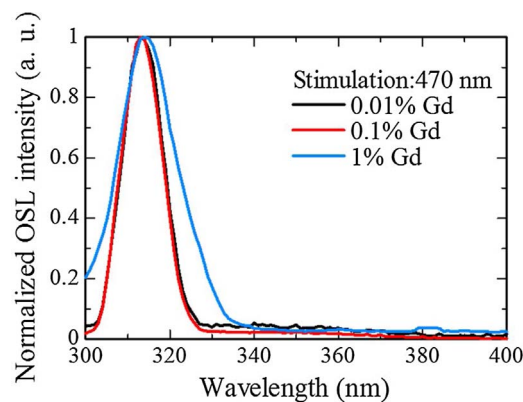
Fig. 11. OSL spectra of MgF$_2$:Gd transparent ceramic samples after 1 Gy X-ray irradiation.
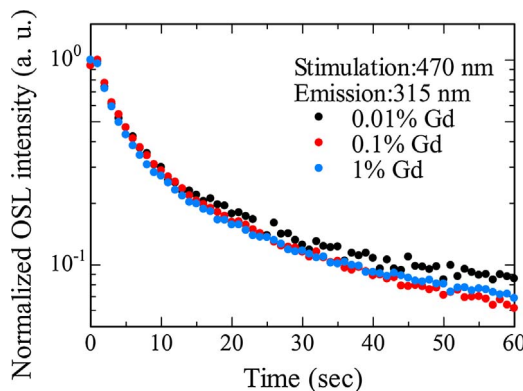
Fig. 12. OSL decay profiles of MgF$_2$ transparent ceramic doped with Gd^{3+} after 1 Gy X-ray irradiation. The monitored emission wavelength was 315 nm while the stimulation wavelength was 470 nm.

energy transfer in addition to excitation/emission processes, which is observed in PL. Therefore, the additional transfer process makes the decay time longer in scintillation.

3.4. Dosimeter properties

Fig. 8 shows TSL glow curves of MgF$_2$:Gd transparent ceramic samples. All the samples showed three glow peaks around 110, 200 and 300 °C. The glow peaks around 110 and 200 °C were also observed in non-doped MgF$_2$ transparent ceramic [37], so the glow peak around 300 °C would be due to some kinds of defects generated by doping with Gd^{3+}. The TSL intensity increased as the Gd concentration increased. This can be because the luminescence intensity was enhanced as observed in scintillation and PL. In addition, the number of defect centers

is supposed to be larger with higher concentration of Gd due to charge imbalance between Gd^{3+} and Mg^{2+}. In addition to the charge imbalance, the impurity phases would enhance the luminescence intensity because the intensity of the 1% Gd-doped sample was considerably higher than that of the other samples. Fig. 9 shows TSL spectra of the MgF_2:Gd transparent ceramic samples. The emission signal was accumulated over a temperature range of 50–350 °C while heating the sample at a rate of 1 °C/s. All the samples showed an intense peak at 310 nm due to the 4f-4f transitions of Gd^{3+}. The host emission around 380 nm was not observed in the TSL unlike the scintillation.

The activation energy and the frequency factors were estimated by TSL glow-curve deconvolution (GCD) functions of general-order kinetics. [38], and the derived values are summarized in Table 2. From the activation energy, it was suggested that Gd^{3+} doping did not influence the trap depths. The frequency factors were smaller than that of the general value (10^{12-13}), so the TSL would be partly caused by the tunneling effect.

Fig. 10 represents dose response curves of the MgF_2:Gd transparent ceramic samples. The TSL intensity was defined as integrated signal over 50–350 °C. The 1% Gd-doped sample showed a good linear response from 0.1–1000 mGy while those of the other samples showed lesser sensitivity by approximately one order of magnitude. The sensitivity of the 1% Gd-doped sample was equivalent to that of commercial personal dosimeters (typical detection limit is 0.1 mGy).

Fig. 11 shows OSL spectra of the MgF_2:Gd transparent ceramic samples. The measurements were carried out after irradiating the samples with X-rays. The stimulation wavelength was 470 nm. All the samples were confirmed to show an OSL emission due to the 4f-4f transitions of Gd^{3+}. The host emission was not observed as in the case of TSL. Since the OSL intensity was weak, we could not accurately measure emission intensities to compare the sensitivities and dose response functions. Fig. 12 represents OSL decay curves of the MgF_2:Gd. The emission was monitored at 310 nm under 470 nm stimulation. The samples were irradiated with X-rays (1 Gy) before the measurements. The decay curves were well-approximated by a second-order exponential function. Therefore, it was suggested that there were at least two de-trapping processes involved in the OSL. The faster decay times of the 0.01, 0.1 and 1% Gd-doped samples were 2.72, 2.50 and 2.31 s, respectively. The slower decay times of the 0.01, 0.1 and 1% Gd-doped samples were 13.31, 13.34 and 12.33 s, respectively. These observations suggest that the Gd-concentration does not strongly influence the OSL processes involved.

4. Conclusions

We have developed MgF_2:Gd transparent ceramics and investigated the scintillation, dosimeter and optical properties. The samples showed an intense scintillation signal with an emission peaking at 310 nm due to the 4f-4f transitions of Gd^{3+} and a broad band around 380 nm from the host matrix under X-ray irradiation. In the TSL, the samples showed an emission due to the 4f-4f transitions of Gd^{3+} while the host emission was not observed. The TSL was very sensitive to X-rays, and the 1% Gd-doped sample showed the highest sensitivity and a good linear response from 0.1 to 1000 mGy. This is an equivalent sensitivity to that of commercial personal dosimeters. Furthermore, the sample also showed OSL emission at 310 nm due to the 4f-4f transitions of Gd^{3+} under 470 nm stimulation.

Acknowledgements

References

[1] T. Ito, T. Yanagida, M. Sato, M. Kokubun, T. Takashima, S. Hirakuri, R. Miyawaki, H. Takahashi, K. Makishima, T. Tanaka, K. Nakazawa, T. Takahashi, T. Honda, A 1-dimensional gamma-ray position sensor based on GSO:Ce scintillators coupled to a Si strip detector, Nucl. Instr. and Meth. A 579 (2007) 239–242.

[2] D. Totsuka, T. Yanagida, K. Fukuda, N. Kawaguchi, Y. Fujimoto, J. Pejchal, Y. Yokota, A. Yoshikawa, Performance test of Si PIN photodiode line scanner for thermal neutron detection, Nucl. Instrum. Methods Phys. Res. Sect. A Accel. Spect. Detect. Assoc. Equip. 659 (2011) 399–402.

[3] T. Yanagida, A. Yoshikawa, Y. Yokota, K. Kamada, Y. Usuki, S. Yamamoto, M. Miyake, M. Baba, K. Kumagai, K. Sasaki, M. Ito, N. Abe, Y. Fujimoto, S. Maeo, Y. Furuya, H. Tanaka, A. Fukabori, T.R. Dos Santos, M. Takeda, N. Ohuchi, Development of Pr:LuAG scintillator array and assembly for positron emission mammography, IEEE Trans. Nucl. Sci. 57 (2010) 1492–1495, http://dx.doi.org/10.1109/TNS.2009.2032265.

[4] M.R. Mayhugh, R.W. Christy, N.M. Johnson, Thermoluminescence and color center correlations in dosimetry LiF, J. Appl. Phys. 41 (1970) 2968–2976, http://dx.doi.org/10.1063/1.1659346.

[5] H. Nanto, A. Nishimura, M. Kuroda, Y. Takei, Y. Nakano, T. Shoji, T. Yanagita, S. Kasai, X-ray imaging plate using CsBr:Eu phosphors for computed radiography, Nucl. Instrum.Methods Phys. Res. Sect. A Accel. Spect. Detect. Assoc. Equip. 580 (2007) 278–281, http://dx.doi.org/10.1016/j.nima.2007.05.155.

[6] T. Yanagida, Y. Fujimoto, K. Watanabe, K. Fukuda, N. Kawaguchi, Y. Miyamoto, H. Nanto, Scintillation and optical stimulated luminescence of Ce-doped CaF$_2$, Radiat. Meas. 71 (2014) 162–165, http://dx.doi.org/10.1016/j.radmeas.2014.03.020.

[7] T. Yanagida, Ionizing radiation induced emission: scintillation and storage-type luminescence, J. Lumin. 169 (2016) 544–548, http://dx.doi.org/10.1016/j.jlumin.2015.01.006.

[8] T. Yanagida, N. Kawaguchi, Y. Fujimoto, K. Fukuda, Y. Yokota, A. Yamazaki, K. Watanabe, J. Pejchal, A. Uritani, T. Iguchi, A. Yoshikawa, Basic study of Europium doped LiCaAlF$_6$ scintillator and its capability for thermal neutron imaging application, Opt. Mater. (Amst.) 33 (2011) 1243–1247, http://dx.doi.org/10.1016/j.optmat.2011.02.016.

[9] D.W. Cooke, Thermoluminescence studies of LiF (TLD-100) in the temperature interval 10–300 K, J. Appl. Phys. 52 (1981) 4244, http://dx.doi.org/10.1063/1.329275.

[10] M. Budzanowski, B. Burgkhardt, P. Olko, W. Pessara, M.P.R. Waligórski, Long-term investigation on self-irradiation and sensitivity to cosmic rays of TL detector types TLD-200, TLD-700, MCP-N and new phosphate glass dosemeter, Radiat. Prot. Dosim. 66 (1996) 135–138 (abstract), http://rpd.oxfordjournals.org/content/66/1-4/135.

[11] C. Furetta, Y. Lee, Further studies of the dosimetric properties of CaF$_2$:Tm (TLD-300), Radiat. Prot. Dosim. 11 (1985) 101–105 (short), http://rpd.oxfordjournals.org/content/11/2/101.

[12] O.E. Facey, W.A. Sibley, Optical absorption and luminescence of irradiated MgF$_2$, Phys. Rev. 186 (1969) 926–932, http://dx.doi.org/10.1103/PhysRev.186.926.

[13] W.A. Sibley, O.E. Facey, Color centers in MgF$_2$, Phys. Rev. 174 (1968) 1076–1082, http://dx.doi.org/10.1103/PhysRev.174.1076.

[14] K. Tanimura, N. Itoh, Lattice instability at excited states of the self-trapped excitons in MgF$_2$, J. Appl. Phys. 69 (1991) 7831, http://dx.doi.org/10.1063/1.347514.

[15] B.C. Hong, K. Kawano, Luminescence studies of the rare earth ions-doped CaF$_2$ and MgF$_2$ films for wavelength conversion, J. Alloys Compd. 408-412 (2006) 838–841, http://dx.doi.org/10.1016/j.jallcom.2005.01.133.

[16] R.T. Williams, C.L. Marquardt, J.W. Williams, M.N. Kabler, Transient absorption and luminescence in MgF$_2$ following electron pulse excitation, Phys. Rev. B 15 (1977) 5003–5011, http://dx.doi.org/10.1103/PhysRevB.15.5003.

[17] M. Secu, S. Jipa, C.E. Secu, T. Zaharescu, R. Georgescu, M. Cutrubinis, Processes involved in the high-temperature thermoluminescence of a Mn^{2+}-doped MgF$_2$ phosphor, Phys. Status Solidi Basic Res. 245 (2008) 159–162, http://dx.doi.org/10.1002/pssb.200743108.

[18] L.G. Jacobsohn, A.L. Roy, C.L. McPherson, C.J. Kucera, L.C. Oliveira, E.G. Yukihara, J. Ballato, Rare earth-doped nanocrystalline MgF$_2$: synthesis, luminescence and thermoluminescence, Opt. Mater. 35 (2013) 2461–2464, http://dx.doi.org/10.1016/j.optmat.2013.06.045.

[19] A. Kumar, D.K. Rai, S.B. Rai, Luminescence of Gd^{3+} ions doped in oxyfluoroborate glass, Solid State Commun. 117 (2001) 387–392, http://dx.doi.org/10.1016/S0038-1098(00)00430-0.

[20] T. Yanagida, K. Kamada, Y. Fujimoto, H. Yagi, T. Yanagitani, Comparative study of ceramic and single crystal Ce:GAGG scintillator, Opt. Mater. 35 (2013) 2480–2485, http://dx.doi.org/10.1016/j.optmat.2013.07.002.

[21] T. Yanagida, K. Kamada, Y. Fujimoto, Y. Yokota, A. Yoshikawa, H. Yagi, T. Yanagitani, Scintillation properties of transparent ceramic and single crystalline Nd:YAG scintillators, Nucl. Instrum. Methods Phys. Res. Sect. A Accel. Spectr. Detect. Assoc. Equip. 631 (2011) 54–57, http://dx.doi.org/10.1016/j.nima.2010.12.038.

[22] P. Palmero, B. Bonelli, G. Fantozzi, G. Spina, G. Bonnefont, L. Montanaro, J. Chevalier, Surface and mechanical properties of transparent polycrystalline YAG fabricated by SPS, Mater. Res. Bull. 48 (2013) 2589–2597, http://dx.doi.org/10.1016/j.materresbull.2013.03.003.

[23] C. Wang, Z. Zhao, Transparent polycrystalline ruby ceramic by spark plasma sintering, Mater. Res. Bull. 45 (2010) 1127–1131, http://dx.doi.org/10.1016/j.materresbull.2010.05.034.

[24] T. Kato, G. Okada, T. Yanagida, Dosimetric properties of Y-doped MgO transparent ceramics, Rad. Meas. (2017), http://dx.doi.org/10.1016/j.radmeas.2017.03.022 in press.

[25] T. Kato, G. Okada, T. Yanagida, Dosimeter properties of CaO transparent ceramic prepared by the SPS method, J. Mater. Sci.-Master. El. 28 (2017) 7018–7023, http://dx.doi.org/10.1007/s10854-016-6024-x.

[26] T. Kato, G. Okada, K. Fukuda, T. Yanagida, Development of BaF$_2$ transparent ceramics and evaluation of the scintillation properties, Radiat. Meas. (2017), http://dx.doi.org/10.1016/j.radmeas.2017.03.032 (in press).

[27] T. Kato, G. Okada, T. Yanagida, Dosimeter properties of MgO transparent ceramic doped with C, Radiat. Meas. 92 (2016) 93–98, http://dx.doi.org/10.1016/j.radmeas.2016.07.004.

[28] T. Kato, G. Okada, T. Yanagida, Optical, scintillation and dosimeter properties of MgO transparent ceramic and single crystal, Ceram. Int. 42 (2016) 5617–5622, http://dx.doi.org/10.1016/j.ceramint.2015.12.070.

[29] T. Kato, G. Okada, T. Yanagida, Optical, scintillation and dosimeter properties of MgO translucent ceramic doped with Cr^{3+}, Opt. Mater. 54 (2016) 134–138, http://dx.doi.org/10.1016/j.optmat.2016.02.030.

[30] T. Kato, G. Okada, T. Yanagida, Optical, scintillation and dosimeter properties of MgO transparent ceramic doped with Mn^{2+}, J. Ceram. Soc. Jpn. 124 (2016) 559–563, http://dx.doi.org/10.2109/jcersj2.15229.

[31] F. Nakamura, T. Kato, G. Okada, N. Kawaguchi, K. Fukuda, T. Yanagida, Scintillation and dosimeter properties of CaF$_2$ translucent ceramic produced by SPS, J. Eur. Ceram. Soc. 37 (2017) 1707–1711, http://dx.doi.org/10.1016/j.jeurceramsoc.2016.11.016.

[32] F. Nakamura, G. Kato, N. Kawaguchi, K. Fukuda, T. Yanagida, Scintillation and dosimeter properties of CaF$_2$ transparent ceramic doped with Eu^{2+}, Ceram. Int. 43 (2017) 604–609.

[33] T. Yanagida, Y. Fujimoto, T. Ito, K. Uchiyama, K. Mori, Development of X-ray-induced afterglow characterization system, Appl. Phys. Express 7 (2014) 8–11, http://dx.doi.org/10.7567/APEX.7.062401.

[34] T. Yanagida, Y. Fujimoto, N. Kawaguchi, S. Yanagida, Dosimeter properties of AlN, J. Ceram. Soc. Japan 121 (2013) 988–991, http://dx.doi.org/10.2109/jcersj2.121.988.

[35] E.H. Penilla, Y. Kodera, J.E. Garay, Simultaneous synthesis and densification of transparent, photoluminescent polycrystalline YAG by current activated pressure assisted densification (CAPAD), Mater. Sci. Eng. B Solid-State Mater. Adv. Technol. 177 (2012) 1178–1187, http://dx.doi.org/10.1016/j.mseb.2012.05.026.

[36] Y. Xu, M. Yamazaki, P. Villars, Inorganic materials database for exploring the nature of material, Jpn. J. Appl. Phys. 50 (2011) http://dx.doi.org/10.1143/JJAP.50.11RH02 (11RH02-11RH5).

[37] F. Nakamura, T. Kato, G. Okada, N. Kawaguchi, K. Fukuda, T. Yanagida, Scintillation, TSL and RPL properties of MgF$_2$ transparent ceramic and single crystal, Ceram. Int. 43 (2017) 7211–7215, http://dx.doi.org/10.1016/j.ceramint.2017.03.009.

[38] G. Kitis, J.M. Gomez-Ros, J.W.N. Tuyn, Thermoluminescence glow-curve deconvolution functions for first, second and general orders of kinetics, J. Phys. D. Appl. Phys. 31 (1998) 2636–2641, http://dx.doi.org/10.1088/0022-3727/31/19/037.